Structural studies of two rhinovirus serotypes complexed with fragments of their cellular receptor

Prasanna R.Kolatkar[1], Jordi Bella[2], Norman H.Olson, Carol M.Bator, Timothy S.Baker and Michael G.Rossmann[3]

Department of Biological Sciences, Purdue University, West Lafayette, IN 47907-1392, USA

[1]Present address: BioInformatics Centre, National University Hospital, National University of Singapore, Singapore 119074
[2]Present address: School of Biological Sciences, University of Manchester, Manchester M13 9PT, UK

[3]Corresponding author
e-mail: mgr@indiana.bio.purdue.edu

P.R.Kolatkar and J.Bella contributed equally to this work

Two human rhinovirus serotypes complexed with two- and five-domain soluble fragments of the cellular receptor, intercellular adhesion molecule-1, have been investigated by X-ray crystallographic analyses of the individual components and by cryo-electron microscopy of the complexes. The three-dimensional image reconstructions provide a molecular envelope within which the crystal structures of the viruses and the receptor fragments can be positioned with accuracy. The N-terminal domain of the receptor binds to the rhinovirus 'canyon' surrounding the icosahedral 5-fold axes. Fitting of molecular models into the image reconstruction density identified the residues on the virus that interact with those on the receptor surface, demonstrating complementarity of the electrostatic patterns for the tip of the N-terminal receptor domain and the floor of the canyon. The complexes seen in the image reconstructions probably represent the first stage of a multistep binding process. A mechanism is proposed for the subsequent viral uncoating process.
Keywords: cryo-EM/crystallography/ICAM-1/receptor specificity/rhinoviruses

Introduction

Human rhinoviruses (HRVs), a genus of the *Picornaviridae* family, are the most frequent etiological agents of common colds (Rueckert, 1996). Rhinoviruses are small, icosahedral viruses, with an average diameter of 300 Å and a molecular mass of ~8.5 $\times$ 10^6 Da. They are composed of a protein shell that encapsidates a single, positive RNA strand of ~7000 bases. The capsid is built from 60 copies each of four viral proteins. The three larger proteins, VP1, VP2 and VP3 (~250 amino acids, 30 kDa each), form the external surface of the virus, whereas VP4 (70 amino acids, 6 kDa) is an internal protein located at the interface between the capsid and genome (Rossmann *et al*., 1985).

With >100 different serotypes identified to date, HRVs exhibit remarkable antigenic variability. To produce infec-tion, HRVs must first attach to a cellular receptor. The major group of HRVs, consisting of ~90 serotypes, utilizes the cell surface glycoprotein, intercellular adhesion molecule-1 (ICAM-1), as its receptor (Greve *et al*., 1989; Staunton *et al*., 1989). A minor group of ~10 HRV serotypes uses members of the low-density lipoprotein receptor family to attach to cells (Marlovits *et al*., 1998).

ICAM-1 belongs to the immunoglobulin (Ig) super-family of cell adhesion molecules, whose defining charac-teristic is an extracellular tandem of Ig-like domains. Up to five different ICAM receptors have been reported to date, which differ in the number of Ig domains, cell type, expression regulation, etc. All share some degree of amino acid sequence homology among corresponding Ig domains and a cell adhesion function. The Ig superfamily also includes many other cell surface determinants, such as CD2, CD4, CD8 and the poliovirus receptor (PVR), some of which are also subverted for cellular recognition and entry by diverse pathogens.

ICAM-1 normally functions to promote intercellular adhesion and signaling, mainly in processes derived from response to inflammation (van de Stolpe and van der Saag, 1996). ICAM-1 is also exploited by human pathogens. For instance, erythrocytes infected by the malarial parasite *Plasmodium falciparum* gain the ability to bind ICAM-1 on the surface of endothelial cells (Berendt *et al*., 1992; Ockenhouse *et al*., 1992). This cytoadherence is used by infected erythrocytes to sequester themselves in tissues, such as the brain, thus minimizing exposure of the parasite to immune surveillance. As an HRV receptor, ICAM-1 localizes the virus near the cellular membrane and triggers the conformational changes in the viral capsid that initiate uncoating, the process by which RNA is released into the cell. Such changes have been described in detail for the analogous interaction of poliovirus (PV) with its receptor PVR (Racaniello, 1996).

High-resolution crystal structures of several HRV sero-types have been reported previously (Rossmann *et al*., 1985; Kim *et al*., 1989; Oliveira *et al*., 1993; Zhao *et al*., 1996; N.Verdaguer, D.Blaas and I.Fita, in preparation). In all these structures, a surface depression or 'canyon', ~12 Å deep and 12–15 Å wide, surrounds each pentagonal vertex of the icosahedral shells. Amino acid residues at the base of the canyon are more conserved than residues exposed elsewhere on the viral surface (Rossmann and Palmenberg, 1988), whereas hypervariable surface res-idues coincide with the binding sites of neutralizing monoclonal antibodies (Sherry *et al*., 1986). It was first suggested (Rossmann *et al*., 1985) and then shown (Olson *et al*., 1993) that the canyon is the receptor attachment site. Mutational analyses of specific residues in the canyon are consistent with its involvement in receptor binding (Colonno *et al*., 1988), and the cryo-electron microscopy (cryo-EM) reconstruction of a complex of HRV16 with

the two N-terminal domains of ICAM-1 (D1D2, residues 1–185) demonstrated that the receptor fragment binds to the central part of the HRV canyon (Olson *et al.*, 1993). When the structure of the D1D2 fragment of ICAM-1 (ICAM-1 D1D2) was determined by X-ray crystallography (Bella *et al.*, 1998; Casasnovas *et al.*, 1998b), it was possible to build a molecular model for the cryo-EM reconstructions by combining the X-ray structures of the different components as constrained by the molecular envelope defined by the cryo-EM density map. Preliminary results (Olson *et al.*, 1993; Bella *et al.*, 1998) indicated that the tip of the ICAM-1 N-terminal domain (D1) makes contact with the canyon floor of HRV16, consistent with mutational data (Staunton *et al.*, 1990; McClelland *et al.*, 1991; Register *et al.*, 1991). Analysis of the charge distribution on the two interacting surfaces showed complementarity, but it was not immediately clear why ICAM-1 is recognized only by major-group HRVs.

A hydrophobic pocket in the center of the VP1 β-barrel lies directly beneath the canyon floor. This pocket has been shown to be the binding site for certain antiviral compounds that inhibit the replication of HRVs and related picornaviruses (Fox *et al.*, 1986; Smith *et al.*, 1986). Furthermore, many major-group HRVs have reduced affinity for HeLa cell membrane attachment when an antiviral compound fills the pocket (Pevear *et al.*, 1989).

In the crystal structures of HRV14 and HRV3, this pocket is empty (Rossmann *et al.*, 1985; Zhao *et al.*, 1996) and in a 'closed' conformation. Crystal structures of HRV14 and HRV3 complexed with antiviral compounds show extensive conformational changes relative to the native structures in the region that separates the pocket from the canyon and raises the canyon floor by 4 Å to accommodate an antiviral compound (Smith *et al.*, 1986). A similar hydrophobic pocket contains uncharacterized lipid-like molecules ('pocket factors') in the crystal structures of PV (Hogle *et al.*, 1985), HRV1A (Kim *et al.*, 1989), HRV16 (Oliveira *et al.*, 1993), coxsackievirus B3 (Muckelbauer *et al.*, 1995), and bovine enterovirus (Smyth *et al.*, 1995). The pocket in each of these structures has an 'open' conformation similar to that observed in the complexes of HRV14 with antiviral drugs. It has been suggested that pocket factors contribute to the thermal stability of the virus and that they are displaced when major-group HRVs attach to ICAM-1 by depressing the canyon floor towards the closed pocket conformation found in HRV14. Loss of pocket factor would then be expected to destabilize the virus and initiate uncoating (Oliveira *et al.*, 1993; Rossmann, 1994).

Receptor attachment initiates early events in the viral life cycle, including entry of the virus into the cell. Ultimately, receptors must mediate passage of viral RNA through a lipid bilayer into the cytoplasm (Rueckert, 1996). HRVs and PVs undergo several progressive transformations when bound to cells. Infectious virions, with sedimentation coefficients of ~150S, are thought to uncoat through intermediate 125S ('A' or altered) particles characterized by the loss of VP4 and the externalization of the N-termini of VP1 (Fricks and Hogle, 1990). Release of RNA leads to the presence of 80S empty capsids. Most 125S and all 80S particles end up as non-infective, abortive products, and only a small fraction of 125S particles attach

to membranes and successfully deliver the viral RNA into the host cell cytoplasm (Rueckert, 1996).

Soluble receptors have been used to reproduce *in vitro* some of the events described above (Koike *et al.*, 1992; Hoover-Litty and Greve, 1993; Yafal *et al.*, 1993). The addition of soluble receptors to PV or HRV produces complexes that dissociate reversibly at low temperature. At higher temperatures, these complexes convert into subparticles analogous to those seen in cell-binding studies (Hoover-Litty and Greve, 1993).

Considerable experimental data now exist that relate to the mechanisms by which ICAM-1 binding to HRVs triggers virus destabilization and uncoating: (i) antiviral compounds bound to the hydrophobic pocket in VP1 inhibit uncoating in HRVs and PVs (Fox *et al.*, 1986); (ii) these antiviral compounds preclude cell binding in many of the major-group HRVs (Pevear *et al.*, 1989, 1992); (iii) HRV antiviral escape mutants may change residues either at the surface of the canyon or in the hydrophobic pocket, thereby increasing the affinity of the virus for its receptor in the first case or decreasing the affinity of antiviral compounds for the virus in the second case (Hadfield *et al.*, 1995); (iv) HRV14 is able to externalize both VP4 and the N-terminus of VP1 in a spontaneous, probably reversible manner ('breathing'), as shown by limited proteolysis followed by mass spectroscopy (Lewis *et al.*, 1998); (v) antibodies against internal epitopes on VP1 and VP4 cause PV neutralization, also suggesting a breathing mechanism for PVs (Li *et al.*, 1994); (vi) HRV14 breathing is largely inhibited by antiviral compounds (Lewis *et al.*, 1998); (vii) there is kinetic evidence for two binding modes of ICAM-1 on the surface of HRVs (Casasnovas and Springer, 1995); and (viii) complexes between HRVs and soluble receptors can be obtained as stable entities, visualized by cryo-EM, and then triggered into an irreversible uncoating step by changes in temperature, pH or receptor concentration (Hoover-Litty and Greve, 1993; Olson *et al.*, 1993). In spite of all this information, however, the precise details of the interaction between HRVs and ICAM-1 and the sequence of events that lead to uncoating remain to be characterized.

Here we report cryo-EM reconstruction analyses of HRV14 and HRV16 complexed with various ICAM-1 fragments. HRV14 dissociates completely in a few minutes when incubated at room temperature with soluble, truncated fragments of ICAM-1 (Hoover-Litty and Greve, 1993), while HRV16 remains stable for several hours under the same conditions. Thus, the earlier cryo-EM analysis of the binding of ICAM-1 to HRV was performed with HRV16 (Olson *et al.*, 1993). The cryo-EM results on the binding of ICAM-1 D1D2 to the less stable HRV14 are presented here, from experiments carried out at 4°C, and compared with an improved analysis of the complex between HRV16 and ICAM-1 D1D2. Additionally, the reconstructions of complexes of HRV16 with the five-domain fragment D1–D5 of ICAM-1, as well as with a mutated version of ICAM-1 D1D2 with reduced glycosylation, are also reported. Molecular models for HRV14, HRV16 and ICAM-1 fragments, available from X-ray crystallographic analyses, have been placed into the cryo-EM reconstructions using automatic fitting procedures. The difference between glycosylated and unglycosyl-

Table I. Different ICAM-1 fragments mentioned in the text

Type	Residues	Domains	Mutations	Expression system	Glycosylation[a]	Crystal structure	PDB i.d. code
1	1–185	D1–D2	wild type	CHO cells	full, complex	this work	1D3L
2	1–185	D1–D2	N103→Q N118→Q N156→Q	baculovirus-infected Sf9 cells	reduced, complex	Bella *et al.* (1998)	1IAM
3[b]	1–190	D1–D2	wild type	modified CHO cells Lec3.2.8.1[c]	full, high-mannose	Casasnovas *et al.* (1998b)	1IC1
4	1–453	D1–D5	wild type	CHO cells	full, complex	–	–

[a]The Asn to Gln mutations in type 2 ICAM-1 remove three out of four glycosylation sites in ICAM-1 D2; the mutant CHO cell line used for type 3 ICAM-1 expression produces mannose-only glycans with reduced heterogeneity.
[b]Two independent molecules per crystallographic asymmetric unit, referred to as A and B.
[c]Casasnovas *et al.* (1998b).

ated forms of ICAM-1 helped to orient and position the receptor molecule correctly in the EM density. Based on these results, we propose a mechanism for how the interaction of HRV with ICAM-1 might initiate uncoating of the viral RNA. The structures of the various HRV–ICAM-1 complexes show that ICAM-1 recognizes slightly different areas of the HRV14 or HRV16 canyon surface, while maintaining a few key interaction patterns that are consistent with the differentiation between major- and minor-group HRVs.

Results and discussion

Flexibility between domains D1 and D2 of ICAM-1

The structure of a mostly deglycosylated ICAM-1 D1D2 fragment (residues 1–185, type 2, Table I) was reported previously by Bella *et al.* (1998). The structure of a slightly longer, fully glycosylated form (residues 1–190, type 3, Table I) has also been published (Casasnovas *et al.*, 1998b). Crystals of fully glycosylated ICAM-1 D1D2 (residues 1–185, type 1, Table I) were obtained previously (Kolatkar *et al.*, 1992), but the structure could not be solved *ab initio* because of the large variability of the unique trigonal axis. However, the availability of the type 2 crystal structure has now permitted the fully glycosylated type 1 structure to be solved by molecular replacement to ~2.8 Å resolution and is reported here.

The structure of the two Ig-like domains (each Ig domain has β-strands A, B,..., G) has a total length of ~75 Å. Each domain has a diameter of ~20 Å, with an interdomain ('elbow') angle of ~150° between the major axes of the two domains. There is an additional disulfide bond, compared with the classical intermediate Ig-type domain (Harpaz and Chothia, 1994), between Cys25 and Cys69 connecting the BC and FG loops in domain D1. Domain D2 has a fold homologous to that of a C-2 Ig domain (Harpaz and Chothia, 1994).

There are four independent versions of the two-domain ICAM-1 fragment in the three available ICAM-1 D1D2 crystal structures (Table I), each with a different elbow angle. This variation in the D1–D2 elbow angle occurs mostly in one plane (Figure 1). This restricted variation exists even though the crystal packing environments and glycosylation properties differ. The lack of a spacer region between the two domains, which permits several close interactions, appears to be the basis of the restricted flexibility. The long FG loop in domain D2 interacts with residues in the βA and βG strands of domain D1.
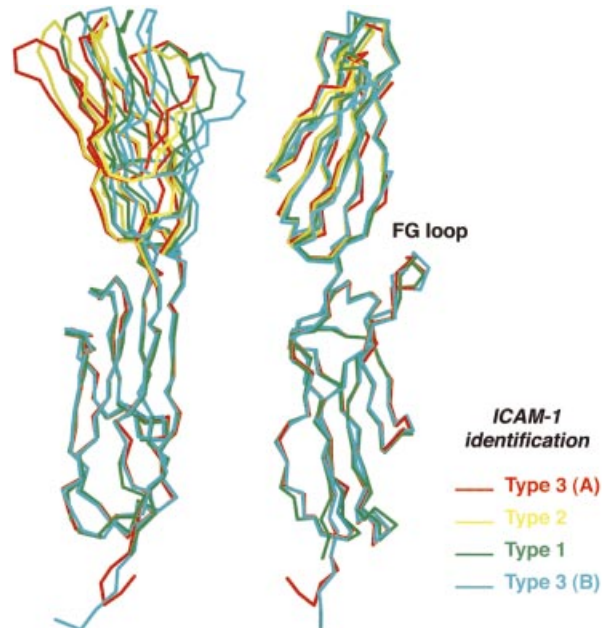

Fig. 1. Variation of the elbow angle between domains D1 and D2 in the crystallographically determined structures of ICAM-1 (Table I). The D2 domains have been aligned in two orthogonal views.

Additionally, there is a salt bridge between residues Arg13 and Glu87 (Bella *et al.*, 1998; Casasnovas *et al.*, 1998b). The average C_α–C_α distance between these two residues in all four ICAM-1 structures is 12.4 ± 0.2 Å. Side chains from residues Ile10, Tyr83, Thr85, Pro115, Asn118, Leu163, Leu165, Gln168, Leu170 and Phe173 define a hydrophobic cushion (Wang and Springer, 1998) that fills the gap between D1 and the FG loop in domain D2. This oily cushion probably allows limited interdomain movement over the surface of the more rigid FG loop.

Cryo-EM reconstructions

The cryo-EM images of the HRV14–type 1 ICAM-1, HRV16–type 2 ICAM-1 and HRV16–type 4 ICAM-1 complexes show 300 Å diameter particles decorated with radially projecting spikes. Complexes between HRV14 and type 1 ICAM-1 are quite unstable (Hoover-Litty and Greve, 1993; Olson *et al.*, 1993) and exist for relatively short incubation periods at 4°C (see Materials and methods). Images of HRV16–type 2 ICAM-1 indicate a greater tendency of these complexes to aggregate com-
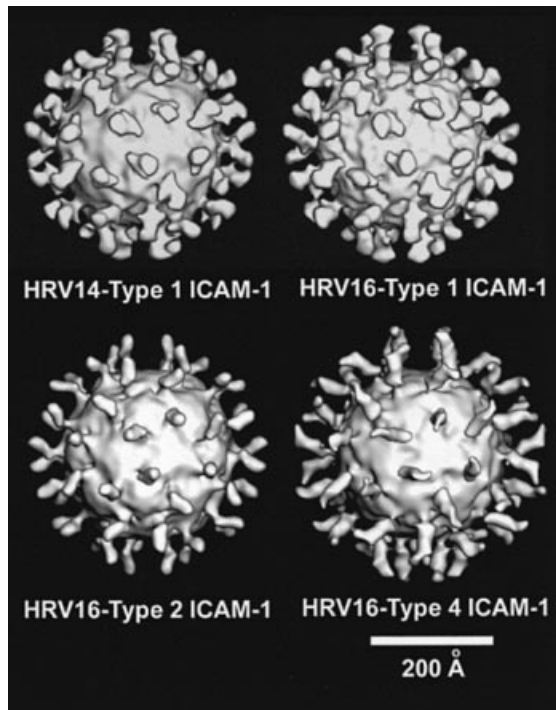
Fig. 2. Cryo-EM image reconstructions of complexes between HRV14 or HRV16 and different soluble fragments of ICAM-1 (see Table I for nomenclature and Table II for statistics). The occupancy of the type 2 and type 4 ICAM-1 fragments is lower, causing them to look thinner at the contour level appropriate for the virus density.

Table II. Cryo-EM image reconstruction statistics of HRV–receptor complexes

Virus ICAM-1[a]	HRV14 Type 1	HRV16 Type 1	HRV16 Type 2	HRV16 Type 4
Underfocus (μm)	1.25	1.0	1.25	1.0
Nominal pixel size (Å)	5.1	5.1	3.9	5.1
No. of particles	36	44	94	23
Effective resolution (Å)	26	28	26	28
ICAM-1 occupancy (%)	85	100	70	60

[a]See Table I for definition of ICAM-1 types.

pared with complexes between HRV14 or HRV16 with the fully glycosylated type 1 ICAM-1.

The image reconstructions (Table II, Figure 2) are similar to those previously reported for HRV16–type 1 ICAM-1 (Olson *et al.*, 1993; Bella *et al.*, 1998). They show viral particles decorated with 60 thumb-like projections, located on the canyon depressions around the 5-fold icosahedral axes. The radii of the features in the virus–receptor complexes range from 150 Å at the virus surface to ~215 Å at the tip of the ICAM-1 D1D2 projections in the type 1 and type 2 reconstructions and to ~250 Å, corresponding to the end of the D3 domain, in the HRV16–type 4 ICAM-1 reconstruction.

Comparison between the electron density values in the ICAM-1 and the virus capsid gives an estimate of the ICAM-1 occupancy in each complex and also an estimate of the conservation of icosahedral symmetry. Whereas occupancy is 100% in the HRV16–type 1 reconstructions, the other three reconstructions show lower occupancies (Table II). No density for domains D4 and D5 appears in
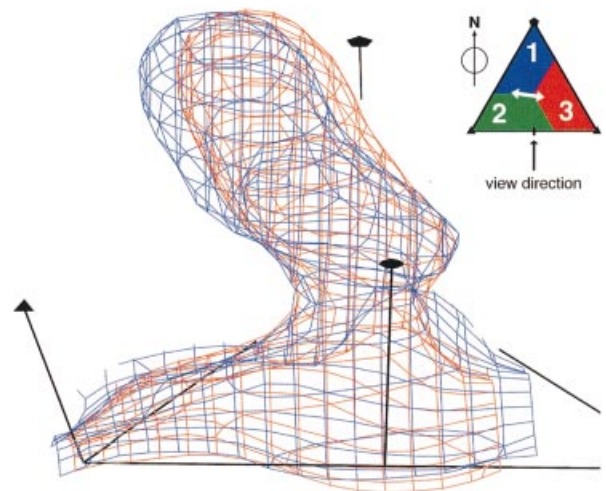

Fig. 3. The cryo-EM reconstructions for HRV16–type 1 ICAM-1 (in red) and HRV14–type 1 ICAM-1 (in blue) depicting the density corresponding to the ICAM-1 fragments. The positions of the icosahedral symmetry elements are shown. A small angular difference indicates a slightly different binding of ICAM-1 to each serotype. The main direction of variation is depicted schematically with a white arrow in the asymmetric unit representation (inset), roughly parallel to the canyon depression. The edge of the canyon nearest to the 5-fold axis is defined as the 'north wall'. The positions of VP1 (blue), VP2 (green) and VP3 (red) are also shown diagrammatically.

the HRV16–type 4 ICAM-1 reconstruction. The apparent occupancy of the D3 domain is lower than that of D1 and D2, indicating that D3 only maintains partial icosahedral symmetry in its complex with HRV16, whereas D4 and D5 retain no icosahedral order. The apparent flexibility of the ICAM-1 molecule beyond domain D3 is consistent with immunolabeling and electron microscopy of individual ICAM-1 molecules (Kirchhausen *et al.*, 1993).

Densities representing the two-domain ICAM-1 molecules in the different reconstructions are similar in shape and orientation, but differ in quality (Table II). The ICAM-1 density in HRV14–type 1 ICAM-1 is tilted ~10° with respect to the corresponding density in HRV16–type 1 ICAM-1 (Figure 3). However, type 1 and type 2 ICAM-1 fragments bind to HRV16 in almost identical orientations.

Identification of the glycosylation sites in the HRV16–type 1 and type 2 ICAM-1 reconstructions

One conspicuous feature in all the cryo-EM reconstructions of HRV–ICAM-1 complexes is the presence of protuberances, or 'lumps', on the ICAM-1 spikes. Such lumps are approximately perpendicular to the long axis of the ICAM-1 molecules (Figure 2). Biochemical data indicate that the tip of domain D1 contains the virus-binding surface. With this orientation of the ICAM-1 D1D2 fragment, all the lumps occur in the D2 domain, consistent with D1 having no potential glycosylation sites and D2 having four such sites. Hence, the lumps represent the carbohydrate moieties of the ICAM-1 fragments.

As many as four lumps per spike can be seen in the HRV16–type 1 or HRV14–type 1 ICAM-1 reconstructions (Figure 2). Electron density maps calculated to 20–25 Å resolution from a molecular model of type 2 ICAM-1 with a single, disordered glycan show a very similar density lump protruding from the smooth, elongated elec-
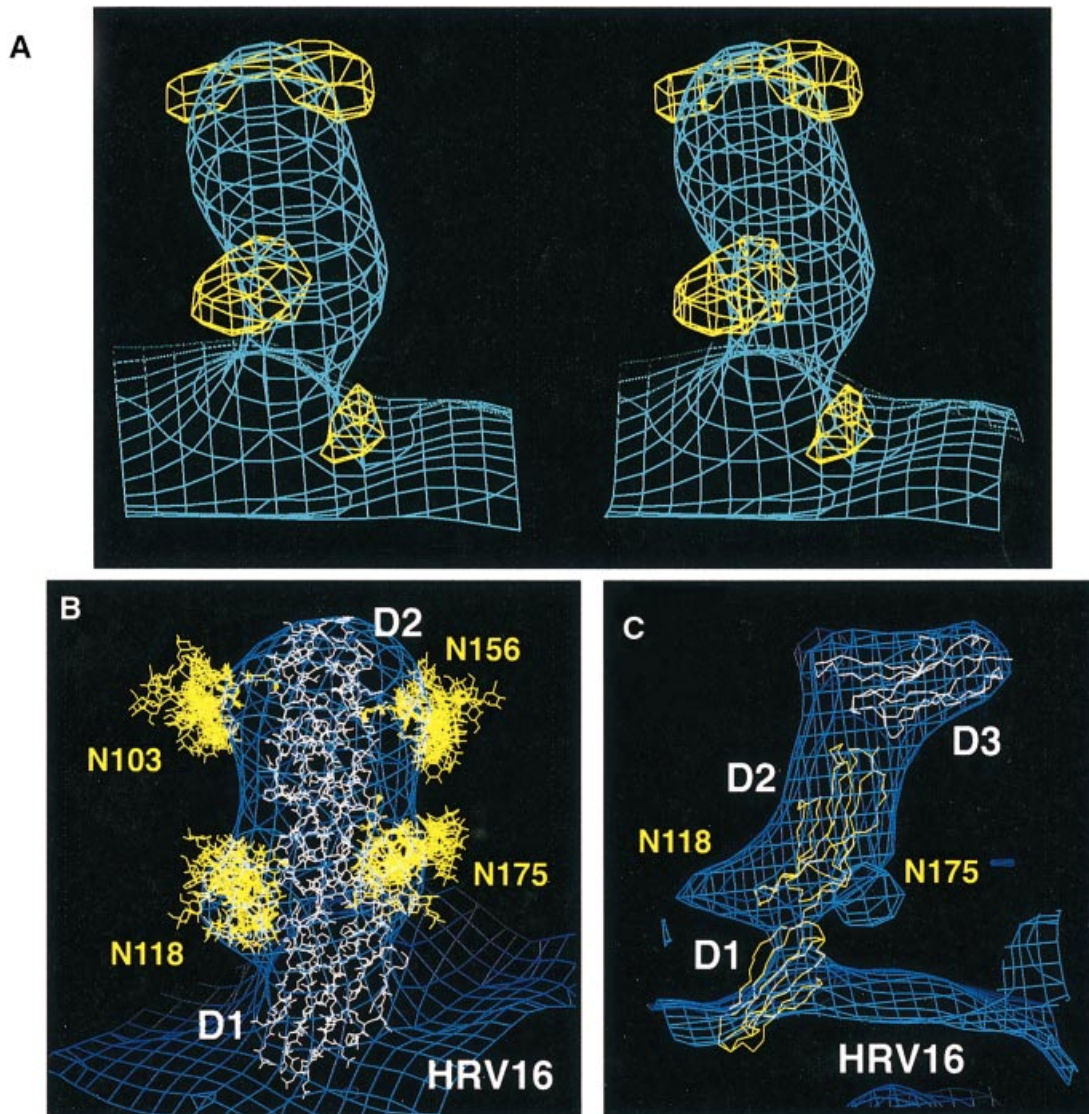
Fig. 4. (A) Stereo diagram of a portion of the HRV16–type 2 ICAM-1 cryo-EM reconstruction corresponding to the density (light blue) for the two-domain ICAM-1 fragment. Superimposed, in yellow, is the difference density map between HRV16–type 1 (fully glycosylated) and HRV16–type 2 (mostly deglycosylated) reconstructions. The density in the HRV16–type 2 reconstruction has been suitably scaled to account for the lower occupancy of the ICAM-1 fragments. **(B)** Fitting of the refined type 1 ICAM-1 model into the cryo-EM reconstruction of the HRV16–type 1 ICAM-1 reconstruction. The protein is represented in white, and the disordered carbohydrates are represented by an ensemble of conformations (yellow). **(C)** A model, represented as a C_α tracing, of D1–D3 of ICAM-1 manually fitted into the HRV16–type 4 ICAM-1 reconstruction. D2 coordinates have been used to model domain D3 of ICAM-1. Additional lumps of electron density correspond to the predicted positions for two carbohydrate moieties on ICAM-1 D2, consistent with the difference density map shown in (A) and the refined ICAM-1 D1D2 model in (B).

tron density (data not shown). A difference cryo-EM density map, computed from the HRV16–type 1 (fully glycosylated) and HRV16–type 2 (partially glycosylated) ICAM-1 reconstructions, shows four areas of significant difference density (Figure 4A). Three of these sites are consistent with three of the density lumps putatively assigned to glycosylation sites. The remaining lump, present in both reconstructions, disappears in the difference map and thus corresponds to the only common glycosylation site, at Asn175. Thus, all four density lumps correspond to carbohydrate moieties on D2.

A small volume of difference density, near the virus surface (Figure 4A), is not compatible with a glycosylation site and might reflect a small change in orientation of ICAM-1 binding between the two complexes.

Fitting of X-ray crystal structures into cryo-EM difference maps

Appropriately glycosylated models of type 1 ICAM-1 with various elbow angles (the angle between the major axis of domain D1 and that of domain D2) were fitted by eye into the cryo-EM electron density maps. Each of the models for the HRV14–type 1 and HRV16–type 1 reconstructions were subsequently refined as rigid bodies in reciprocal space with respect to difference maps obtained by subtraction of the HRV contribution from the cryo-EM reconstructed density of the complexes (J.Bella and M.G.Rossmann, in preparation). The refined fits of the ICAM-1 D1D2 models into the cryo-EM density maps are consistent with the predicted positions of glycosylation (Figure 4B).

The quality of fit, measured with an *R*-factor computed to 28 Å resolution, is comparable for both reconstructions. Given the resolution of the reconstructions, the variation in elbow angle within physically reasonable limits could not be differentiated. Differences in atomic positions among models with different elbow angles were no greater than 5 Å. However, the fit of a given model into the cryo-EM density maps of ICAM-1 complexed with HRV14 or HRV16 was distinguishable. The r.m.s. difference in equivalent C_α positions between the best fits for the HRV16–type 1 and HRV14–type 1 reconstructions was 3.3 Å, corresponding to a 6.8° orientation difference between these two structures. Thus, although it was difficult to pin down the exact elbow angle between domains D1 and D2, it was possible to position domain D1 relative to the virus surface to less than the distance between adjacent C_α atoms.

A model for the three N-terminal domains of type 4 ICAM-1 was built manually into the density of the HRV16–type 4 reconstruction (Figure 4C), using the refined ICAM-1 coordinates for the HRV16–type 1 reconstruction and a copy of D2 as a model for the third domain of ICAM-1. The fitting indicated that there is enough additional density to position ICAM-1 D3. This domain seems to be oriented at ~120° with respect to the major axis of domains D1D2 (Figure 4C). No attempt was made to refine this model.

ICAM-1 footprint on the surfaces of HRVs

The ICAM-1 models with the lowest *R*-factor were used for the analysis of the interactions of type 1 ICAM-1 with HRV14 and HRV16. Coordinates for the viral protein surfaces were obtained from the X-ray structures of HRV14 (Rossmann *et al.*, 1985; Arnold and Rossmann, 1990) and HRV16 (Hadfield *et al.*, 1997). Side chains of residues at the HRV–ICAM-1 interface in each of the complexes were refined to optimize their interactions, using one round of energy minimization. Footprints of type 1 ICAM-1 on the viral surfaces of HRV16 and HRV14 were determined by using distance matrix and buried surface analyses. The calculated area of contact between ICAM-1 and either HRV14 or HRV16 is 990 Å^2. Residues on the surface of HRV16 and HRV14 that become less exposed to the solvent upon complex formation (assuming a probe of 1.4 Å radius) are shown as roadmaps (Chapman, 1993) (Figure 5).

There are no residue contacts between domain D2 of ICAM-1 and the viral surface, in approximate agreement with mutational studies. Also, no contacts are observed between the carbohydrate moieties and the virus, although the long, disordered glycan models potentially are able to reach the virus surface. This lack of contact is consistent with the observation that two-domain ICAM-1 fragments with different degrees of glycosylation bind to HRVs with similar kinetics (Casasnovas *et al.*, 1998a).

Loops BC and FG of domain D1 contact both VP1 and VP3, whereas loop DE only contacts VP1. Loop CD abuts a broad area of VP2, on the 'south' wall of the canyon (see Figure 3) (Bella *et al.*, 1998), and strands βC and βD make additional contacts with some VP1 and VP2 residues. The footprint of ICAM-1 on HRV14 is shifted slightly with respect to the footprint on HRV16. In both complexes, the ICAM-1 footprint includes several of the
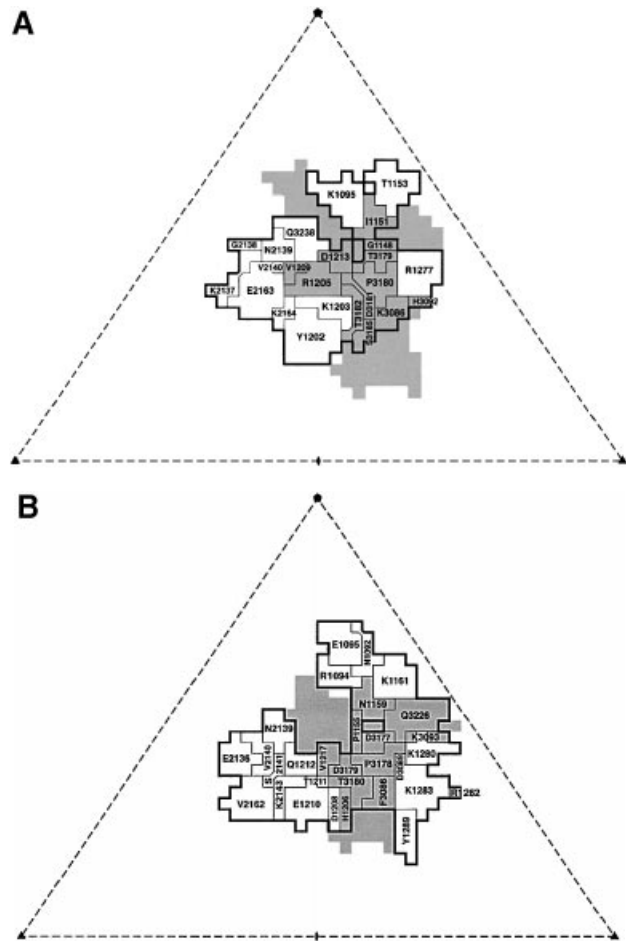

Fig. 5. Roadmap representation (Chapman, 1993) showing the amino acids within the ICAM-1 footprint (thick outline) on the surface of (**A**) HRV16 and (**B**) HRV14. The figure shows one icosahedral asymmetric unit with a 5-fold axis at the top and 3-fold axes to the left and right at the bottom. Residues closer than 145 Å to the viral center, shaded in gray, outline the central and deepest region of the canyon.

residues that define the deepest regions in the canyon surface (Figure 5). Residues Lys1095–Leu1100 and Val1210–Leu1217 in HRV16 define the 'roof' of the hydrophobic drug-binding pocket in VP1 (viral residues are numbered sequentially, starting at 1000, 2000, 3000 and 4000 for the polypeptide chains VP1, VP2, VP3 and VP4, respectively). Of these residues, only Asp1213 makes contact with ICAM-1. Equivalent residues in HRV14, Asp1101–Leu1106 and Val1217–Met1224, are all outside the ICAM-1 footprint when the pocket is closed, and none of them are closer than 4 Å to any ICAM-1 residue. When the pocket is filled by an antiviral compound (Badger *et al.*, 1989), then only His1220 becomes part of the ICAM-1 footprint. Nevertheless, mutations at Lys1103, Val1217, His1220 and Ser1223, in the roof of the hydrophobic pocket in HRV14, all modify the ability of the virus to bind to HeLa cell membranes (Colonno *et al.*, 1988).

Hence, ICAM-1 does not make extensive contacts with the residues that undergo the largest conformational changes when an empty pocket becomes filled with an antiviral compound or pocket factor (see below). Yet, binding studies in the presence of antiviral compounds
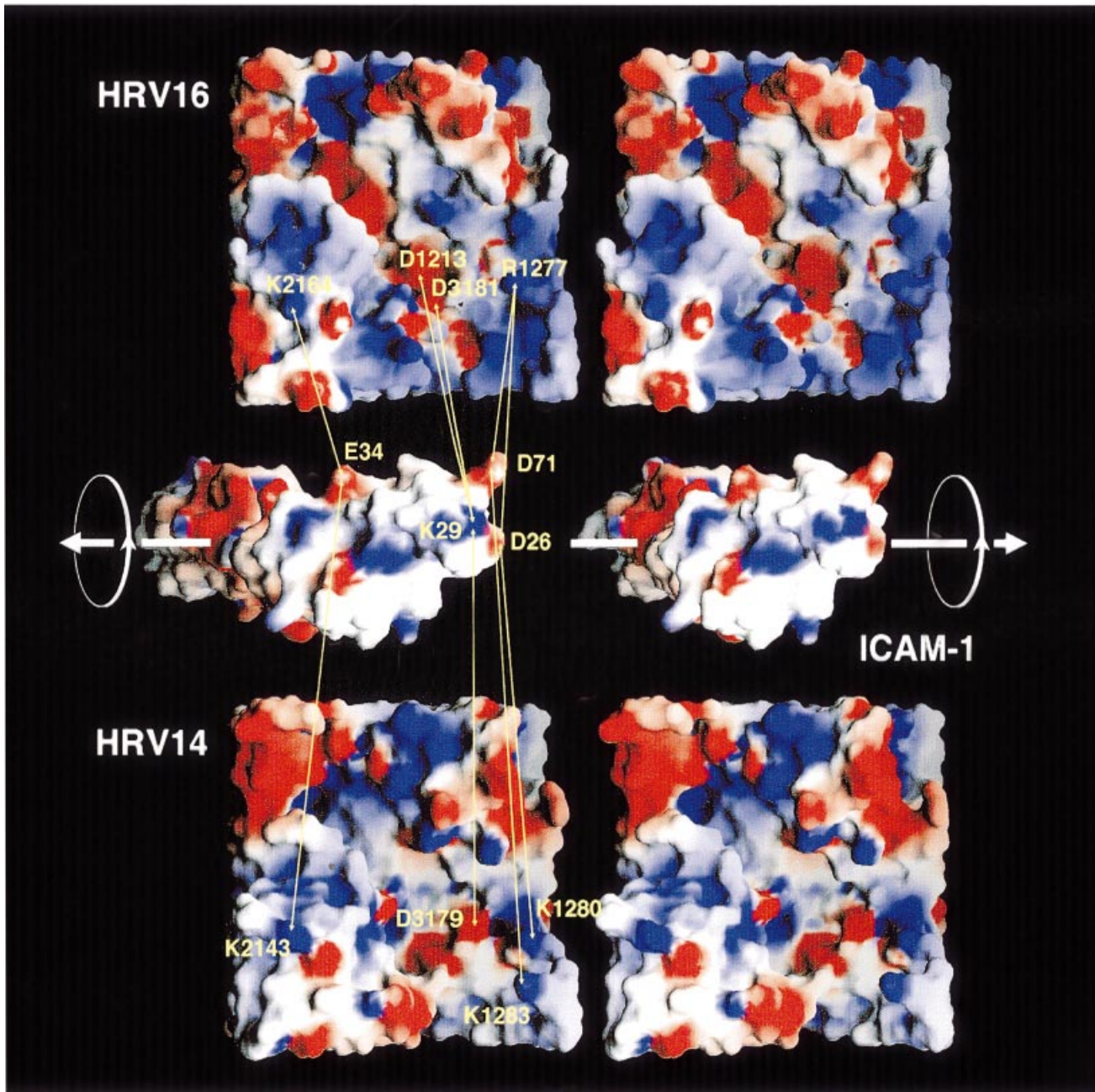
Fig. 6. Stereo representations of electrostatic charge distribution in the canyon region of HRV16 (top), HRV14 (bottom) and the tip of ICAM-1. Charge distributions are represented by the usual colors. Residues that show charge complementarity are indicated and connected with dashed lines.

suggest that the ICAM-1-binding site and the drug-binding site are overlapping and that the binding events are competitive. Thus, the cryo-EM structures appear to be inconsistent with the inhibition of attachment of major-group HRVs to cell membranes when the virus has been inoculated with antiviral compounds (Pevear *et al.*, 1989, 1992), and they are also inconsistent with the mutational results of Colonno *et al.* (1988). A two-step mechanism for ICAM-1 binding, as discussed below, can be invoked to explain how the complex observed by cryo-EM may only represent an initial recognition event and how a subsequent event may lead to a closer association with the virus.

Electrostatic interactions

Charge complementarity exists between the tip of ICAM-1 D1 and the floor of the canyon (Figure 6). Such complementarity is not maintained as a result of residue conservation, but rather by compensating changes of amino acids between serotypes (Table III). Our cryo-EM results show that ICAM-1 can bind in slightly different orientations to different HRV serotypes and still maintain favorable interactions. Two acidic residues in HRV16, Asp1213 and Asp3181, interact with Lys29 of ICAM-1 D1 (Table III). However, in HRV14, only Asp3179 (homologous to Asp3181 in HRV16) opposes Lys29 (Table III). Similarly, Lys2164 on the south wall of HRV16 interacts with Glu34

Table III. Charge complementarity at the HRV–ICAM-1 interface

ICAM-1 Site	Residue	HRV16 Interaction	HRV14 Alignment[a]	HRV14 Interaction	HRV16 Alignment[a]
BC loop	Asp26	Arg1277	Lys1280	Lys1280 Lys1283	Arg1277 Thr1280
BC loop	Lys29	Asp1213 Asp3181	His1220 Asp3179	Asp3179	Asp3181
βC	Glu34	Lys2164	Gly2163	Lys2143	Gly2143
βE	Lys50	VP3 COOH	VP3 COOH		
FG loop	Asp71	Arg1277 Lys3086	Lys1280 Asn3084	Lys1283	Thr1280

HRV residues aligned by Palmenberg (1998).
[a]Equivalent residue in the homologous virus, but not necessarily involved in binding to ICAM-1.

of ICAM-1, whereas in HRV14, Lys2143 faces Glu34 from a different direction (Table III).

HRVs discriminate between ICAM-1 and other homologous molecules, such as ICAM-2 or ICAM-3. This specificity has been rationalized by the crystallographic and sequence analysis of the BC, DE and FG loops in domain D1, which differ in sequence and conformation between the different ICAMs (Bella *et al.*, 1998). Nevertheless, all major-group HRVs show only moderate sequence conservation. Minor-group HRVs, which do not bind ICAM-1, are not obviously distinct from the major-group HRVs. Furthermore, the major-group HRV14 serotype is more distantly related to HRV16 than are the minor-group HRV1A and HRV2 serotypes (Palmenberg, 1998). Nevertheless, the residues that line the canyon of the known minor group serotype structures can be differentiated from those of the major group serotypes (J.Bella, N.Verdaguer, I.Fita and M.G.Rossmann, in preparation).

Possible mechanisms for ICAM-1-induced uncoating

The cryo-EM results described here demonstrate that ICAM-1 makes little contact with the residues that form the roof of the antiviral agent-binding pocket (equivalent to the floor of the canyon). This is inconsistent with previously proposed mechanisms for viral uncoating and cell entry (Rossmann, 1994). Nevertheless, extensive data (see Introduction) link the ability of ICAM-1 to induce uncoating with the conformational state of the pocket. We therefore propose a modified, two-step mechanism (Figure 7), in which the cryo-EM reconstruction of HRVs complexed with soluble ICAM-1 fragments represent the initial recognition event. In a subsequent step, the receptor moves slightly to allow the 'north' wall of the canyon (see Figure 3), consisting of VP1 residues, to bind to domain D1. The resulting conformational change in the virion is envisaged to move VP1 away from the 5-fold axis, thereby opening a channel at the pentamer vertex through which the N-termini of VP1 and VP4, and eventually RNA, can be externalized (Giranda *et al.*, 1992; Rueckert, 1996). There could also be alternative, but less likely, routes for the externalization of VP4, the N-terminus of VP1 and RNA. More than one ICAM-1 molecule might need to be bound to the same pentamer vertex to initiate uncoating. As the genomic RNA lacks icosahedral sym-
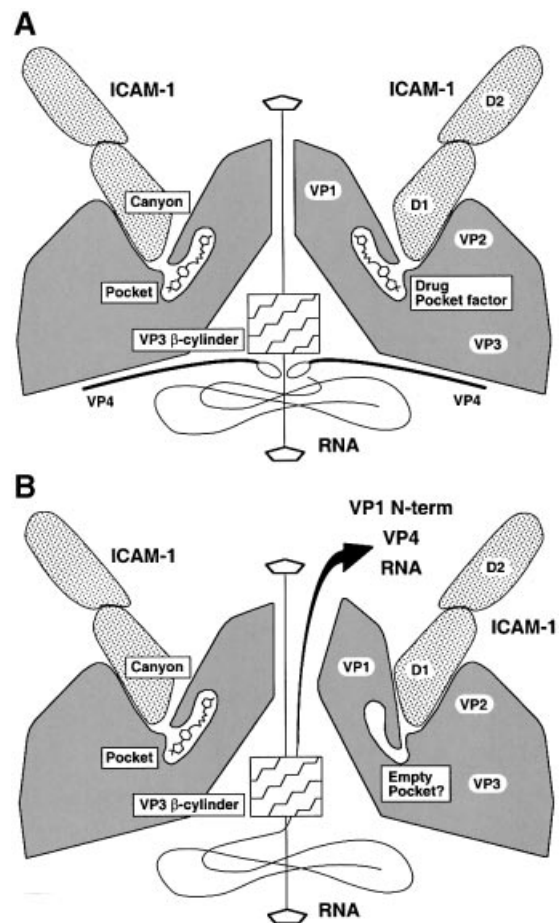

Fig. 7. Schematic representation of a proposed two-step binding mechanism between ICAM-1 and major-group HRVs. ICAM-1 is represented only as a two-domain fragment. (**A**) The first (observed) step corresponds to the cryo-EM reconstructions of HRV—ICAM-1 fragments in which ICAM-1 binds primarily to the floor and south wall of the canyon. (**B**) The second (hypothesized) step involves a conformational change in the virus suface, shown only on the right-hand side of the diagram. Probably both walls of the canyon bind to domain D1 of ICAM-1 and, in so doing, open up the 5-fold channel. This requires conformational flexibility of VP1, which forms a large part of both the north and south walls of the canyon, and probably also an empty hydrophobic pocket in VP1. Opening of the pentamer vertex, induced by the binding of one or more ICAM-1 molecules, may facilitate externalization of VP4 and other internal viral components, including RNA.

metry, only a single pentamer vertex can act as the portal for RNA release.

The area on the floor of the canyon, which makes a tenuous link between the north and south sides of the canyon, may be the hinge region around which VP1 can flex. This area is associated with the antiviral pocket. Antiviral compounds bound to the pocket would stiffen the hinge, thus preventing uncoating (Figure 7B).

A corollary to this mechanism is that, even in the absence of receptor, the viral capsid dynamically opens and closes at the pentamer vertex, thereby permitting normally buried elements, such as VP4s or the N-termini of VP1, to become exposed periodically (Lewis *et al.*, 1998). Such viral breathing may be stimulated progressively as more and more receptors are recruited from the cellular membrane, until irreversible uncoating occurs (Rueckert, 1996).

The two-step mechanism is consistent with the presence on HRV surfaces of two binding modes with different affinity for ICAM-1 (Casasnovas and Springer, 1995), but with only one type being observed in the cryo-EM reconstructions. This would explain why virus can be preserved as a complex for cryo-EM experiments without being converted to empty particles. The initial binding step (as observed here at 4°C) occurs with little contact between ICAM-1 and the canyon floor on top of the pocket. More substantial contacts are made during the subsequent step (at elevated temperatures), probably with residues on the DE loop of ICAM-1 D1, not allowed when a drug is bound.

With a few exceptions, major-group HRVs have reduced affinity for cell membrane attachment when an antiviral compound is in the pocket, although the degree of sensitivity to attachment inhibition can vary dramatically among serotypes (Pevear *et al.*, 1989, 1992). It was proposed that inhibition of binding occurs as a result of the overlap between the binding sites of ICAM-1 and the antiviral compounds. The two-step mechanism would, therefore, suggest that the second step leads to tighter binding. However, such binding is inhibited if breathing is restricted by the presence of antiviral compounds.

The drug-binding pocket is rarely empty in crystal structures of HRVs, coxsackieviruses, PVs and other enteroviruses. It has been suggested that pocket-binding antiviral drugs displace such pocket factors and that competition between pocket factors and receptors regulates the viral stability (Rossmann, 1994). The mechanism proposed in Figure 7 is compatible with the assumption that ICAM-1 ejects weakly bound pocket molecules in the second binding step, but it is unable to remove tightly bound antiviral compounds.

Wild-type HRVs or PVs are capable of extensive breathing (Li *et al.*, 1994; Lewis *et al.*, 1998). However, HRVs with pocket-bound antiviral compounds are prevented from breathing. Presumably, pocket factors present in most of these viruses are able to enter and leave the pocket spontaneously. In contrast, the antiviral compounds bind with higher affinity and, hence, occupy the pocket for a greater percentage of time, effectively inhibiting breathing.

The proposed mechanism is also consistent with the observation that antibodies against the neutralizing immunogenic site IA (NIm-IA) of HRV14, at residues 1091–1095, stabilize the virus against uncoating, whereas antibodies against other antigenic sites in HRV14 do not provide additional stability (Che *et al.*, 1998). In structures of complexes between HRV14 and Fab molecules that bind to NIm-IA (Smith *et al.*, 1996; Che *et al.*, 1998), the Fab regions simultaneously contact the north and south walls of the canyon, thus preventing the VP1 hinge movement (Figure 7B) and, therefore, interfering with uncoating.

Materials and methods

X-ray crystallographic analysis of fully glycosylated ICAM-1 D1D2

Crystallization of type 1 ICAM-1 was reported previously (Kolatkar *et al.*, 1992). X-ray diffraction data were collected to 2.8 Å resolution. The crystals showed very high variability of unit cell dimensions—up to 17% in the length of the crystallographic *c*-axis. This precluded the use of isomorphous replacement methods for the structure determination. However, the genetically engineered form of type 2 ICAM-1 was more amenable to X-ray crystallographic studies (Bella *et al.*, 1998). The resulting coordinates were used to solve the crystal structure of fully glycosylated type 1 ICAM-1 by the molecular replacement method, using the program AMoRe (Navaza, 1994). Rotation functions were calculated independently for domains D1 and D2, and their orientation was determined separately. Translation searches were performed in both $P3_121$ and $P3_221$ space groups, and showed that $P3_121$ was the correct one. Refinement of the structure proceeded through alternate cycles of manual rebuilding with a computer graphics workstation and conjugate gradient minimization, using the programs CHAIN (Sack, 1988) and X-PLOR (Brünger, 1992).

Preparation of HRV–ICAM-1 complexes

HRV14 was incubated with type 1 ICAM-1 for 30 min at 4°C and 5 mg/ml virus concentration, using an 8-fold excess of ICAM-1 for each of the 60 possible binding sites per virion. In contrast, complexes between HRV16 and type 1, type 2 or type 4 ICAM-1 were prepared by incubation of samples for ~16 h at 34°C [types 1 and 4 (Olson *et al.*, 1993)] or room temperature (type 2), using a 16-fold (types 1 and 4) or 54-fold (type 2) excess of ICAM-1 per binding site.

Cryo-electron microscopy

After incubation, samples were vitrified as described (Olson *et al.*, 1993) and maintained at near liquid nitrogen temperature in Philips EM420 and CM200 electron microscopes with a Gatan 626 cryotransfer holder. Electron micrographs of HRV14–type 1 ICAM-1 complex particles were recorded at 80 kV with minimal dose techniques (<20 e$^-$/Å^2), at a nominal magnification of ×49 000. Electron micrographs of HRV16–type 2 complex particles were recorded at 200 kV, minimal dose, and nominal magnification of ×38 000. Only data from the high defocus images (Table II) were used in this study, thus limiting the final resolution of the reconstruction. Preliminary selection of micrographs, digitization and preparation of complex particle images were performed as described (Olson *et al.*, 1993). The three-dimensional reconstruction of the HRV16–type 1 ICAM-1 complex (Olson *et al.*, 1993) (Table II, Figure 2) was used as the starting model to determine the orientation parameters and centers of density of the selected particle images of the HRV14–type 1 ICAM-1 complex (Baker and Cheng, 1996). For the HRV16–type 2 ICAM-1 complex images, an HRV16 reconstruction was used as a starting model. Subsequent refinement of orientation parameters was performed with reconstructed density maps until no further improvement in the self-consistency of the data was obtained. Data statistics for all the reconstructions are shown in Table II. The effective resolutions of the reconstructions were determined by randomly splitting the data for each reconstruction into two sets and comparing structure factors obtained from separate reconstructions. Eigenvalue spectra give an indication of the randomness of the data that were included in the reconstructions. The completeness of the data was verified in that all eigenvalues exceeded 1.0.

Model fitting

Coordinate fitting was carried out with the program X-PLOR (Brünger, 1992) and the graphics program CHAIN (Sack, 1988). The reproducibility of the refinement process was accurate to <1.5 Å. Thus, the atomic

interaction determined here can be accepted subject to the assumption that the crystallographically determined structures of the virus and receptor fragment are not altered substantially by the formation of the complex. The results presented here will be verified by further experimentation. The program GRASP (Nicholls *et al.*, 1991) was used for electrostatic charge calculations (Figure 6). The X-ray structure coordinates for ICAM-1 D1 (Bella *et al.*, 1998), HRV16 (Hadfield *et al.*, 1997), and HRV14 (Arnold and Rossmann, 1990) were used to compute the electrostatic surface potential.

Data deposition

Coordinates for type 1 ICAM-1 have been deposited with the Protein Data Bank (accession code 1D3L). C_α coordinates of the ICAM-1 D1D2 when docked into HRV14 and HRV16 have also been deposited with the Protein Data Bank (accession codes 1D3I and 1D3E, respectively).

Acknowledgements

References

Arnold,E. and Rossmann,M.G. (1990) Analysis of the structure of a common cold virus, human rhinovirus 14, refined at a resolution of 3.0 Å. *J. Mol. Biol.*, **211**, 763–801.

Badger,J., Minor,I., Oliveira,M.A., Smith,T.J. and Rossmann,M.G. (1989) Structural analysis of antiviral agents that interact with the capsid of human rhinoviruses. *Proteins*, **6**, 1–19.

Baker,T.S. and Cheng,R.H. (1996) A model-based approach for determining orientations of biological macromolecules imaged by cryoelectron microscopy. *J. Struct. Biol.*, **116**, 120–130.

Bella,J., Kolatkar,P.R., Marlor,C.W., Greve,J.M. and Rossmann,M.G. (1998) The structure of the two amino-terminal domains of human ICAM-1 suggests how it functions as a rhinovirus receptor and as an LFA-1 integrin ligand. *Proc. Natl Acad. Sci. USA*, **95**, 4140–4145.

Berendt,A.R., McDowall,A., Craig,A.G., Bates,P.A., Sternberg,M.J.E., Marsh,K., Newbold,C.I. and Hogg,N. (1992) The binding site on ICAM-1 for *Plasmodium falciparum*-infected erythrocytes overlaps, but is distinct from, the LFA-1 binding site. *Cell*, **68**, 71–81.

Brünger,A.T. (1992) *X-PLOR. Version 3.1. A System for X-ray Crystallography and NMR*. Yale University Press, New Haven, CT.

Casasnovas,J.M. and Springer,T.A. (1995) Kinetics and thermodynamics of virus binding to receptor. Studies with rhinovirus, intercellular adhesion molecule-1 (ICAM-1) and surface plasmon resonance. *J. Biol. Chem.*, **270**, 13216–13224.

Casasnovas,J.M., Bickford,J.K. and Springer,T.A. (1998a) The domain structure of ICAM-1 and the kinetics of binding to rhinovirus. *J. Virol.*, **72**, 6244–6246.

Casasnovas,J.M., Stehle,T., Liu,J., Wang,J. and Springer,T.A. (1998b) A dimeric crystal structure for the N-terminal two domains of intercellular adhesion molecule-1. *Proc. Natl Acad. Sci. USA*, **95**, 4134–4139.

Chapman,M.S. (1993) Mapping the surface properties of macromolecules. *Protein Sci.*, **2**, 459–469.

Che,Z., Olson,N.H., Leippe,D., Lee,W., Mosser,A.G., Rueckert,R.R., Baker,T.S. and Smith,T.J. (1998) Antibody-mediated neutralization of human rhinovirus 14 explored by means of cryoelectron microscopy and X-ray crystallography of virus–Fab complexes. *J. Virol.*, **72**, 4610–4622.

Colonno,R.J., Condra,J.H., Mizutani,S., Callahan,P.L., Davies,M.E. and Murcko,M.A. (1988) Evidence for the direct involvement of the rhinovirus canyon in receptor binding. *Proc. Natl Acad. Sci. USA*, **85**, 5449–5453.

Fox,M.P., Otto,M.J. and McKinlay,M.A. (1986) The prevention of rhinovirus and poliovirus uncoating by WIN 51711: a new antiviral drug. *Antimicrob. Agents Chemother.*, **30**, 110–116.

Fricks,C.E. and Hogle,J.M. (1990) Cell-induced conformational change in poliovirus: externalization of the amino terminus of VP1 is responsible for liposome binding. *J. Virol.*, **64**, 1934–1945.

Giranda,V.L., Heinz,B.A., Oliveira,M.A., Minor,I., Kim,K.H.,

Kolatkar,P.R., Rossmann,M.G. and Rueckert,R.R. (1992) Acid-induced structural changes in human rhinovirus 14: possible role in uncoating. *Proc. Natl Acad. Sci. USA*, **89**, 10213–10217.

Greve,J.M., Davis,G., Meyer,A.M., Forte,C.P., Yost,S.C., Marlor,C.W., Kamarck,M.E. and McClelland,A. (1989) The major human rhinovirus receptor is ICAM-1. *Cell*, **56**, 839–847.

Hadfield,A.T. *et al.* (1995) Structural studies on human rhinovirus 14 drug-resistant compensation mutants. *J. Mol. Biol.*, **253**, 61–73.

Hadfield,A.T., Lee,W., Zhao,R., Oliveira,M.A., Minor,I., Rueckert,R.R. and Rossmann,M.G. (1997) The refined structure of human rhinovirus 16 at 2.15 Å resolution: implications for the viral life cycle. *Structure*, **5**, 427–441.

Harpaz,Y. and Chothia,C. (1994) Many of the immunoglobulin superfamily domains in cell adhesion molecules and surface receptors belong to a new structural set which is close to that containing variable domains. *J. Mol. Biol.*, **238**, 528–539.

Hogle,J.M., Chow,M. and Filman,D.J. (1985) Three-dimensional structure of poliovirus at 2.9 Å resolution. *Science*, **229**, 1358–1365.

Hoover-Litty,H. and Greve,J.M. (1993) Formation of rhinovirus-soluble ICAM-1 complexes and conformational changes in the virion. *J. Virol.*, **67**, 390–397.

Kim,S., Smith,T.J., Chapman,M.S., Rossmann,M.G., Pevear,D.C., Dutko,F.J., Felock,P.J., Diana,G.D. and McKinlay,M.A. (1989) Crystal structure of human rhinovirus serotype 1A (HRV1A). *J. Mol. Biol.*, **210**, 91–111.

Kirchhausen,T., Staunton,D.E. and Springer,T.A. (1993) Location of the domains of ICAM-1 by immunolabeling and single-molecule electron microscopy. *J. Leukoc. Biol.*, **53**, 342–346.

Koike,S., Ise,I., Sato,Y., Mitsui,K., Horie,H., Umeyama,H. and Nomoto,A. (1992) Early events of poliovirus infection. *Semin. Virol.*, **3**, 109–115.

Kolatkar,P.R. *et al.* (1992) Preliminary X-ray crystallographic analysis of intercellular adhesion molecule-1. *J. Mol. Biol.*, **225**, 1127–1130.

Lewis,J.K., Bothner,B., Smith,T.J. and Siuzdak,G. (1998) Antiviral agent blocks breathing of the common cold virus. *Proc. Natl Acad. Sci. USA*, **95**, 6774–6778.

Li,Q., Yafal,A.G., Lee,Y.M.H., Hogle,J. and Chow,M. (1994) Poliovirus neutralization by antibodies to internal epitopes of VP4 and VP1 results from reversible exposure of these sequences at physiological temperature. *J. Virol.*, **68**, 3965–3970.

Marlovits,T.C., Abrahamsberg,C. and Blaas,D. (1998) Very-low-density lipoprotein receptor fragment shed from HeLa cells inhibits human rhinovirus infection. *J. Virol.*, **72**, 10246–10250.

McClelland,A., deBear,J., Yost,S.C., Meyer,A.M., Marlor,C.W. and Greve,J.M. (1991) Identification of monoclonal antibody epitopes and critical residues for rhinovirus binding in domain 1 of ICAM-1. *Proc. Natl Acad. Sci. USA*, **88**, 7993–7997.

Muckelbauer,J.K., Kremer,M., Minor,I., Diana,G., Dutko,F.J., Groarke,J., Pevear,D.C. and Rossmann,M.G. (1995) The structure of coxsackievirus B3 at 3.5 Å resolution. *Structure*, **3**, 653–667.

Navaza,J. (1994) AMoRe—an automated package for molecular replacement. *Acta Crystallogr. A*, **50**, 157–163.

Nicholls,A., Sharp,K.A. and Honig,B. (1991) Protein folding and association: insights from the interfacial and thermodynamic properties of hydrocarbons. *Proteins*, **11**, 281–296.

Ockenhouse,C.F., Betageri,R., Springer,T.A. and Staunton,D.E. (1992) *Plasmodium falciparum*-infected erythrocytes bind ICAM-1 at a site distinct from LFA-1, Mac-1 and human rhinovirus. *Cell*, **68**, 63–69.

Oliveira,M.A. *et al.* (1993) The structure of human rhinovirus 16. *Structure*, **1**, 51–68.

Olson,N.H., Kolatkar,P.R., Oliveira,M.A., Cheng,R.H., Greve,J.M., McClelland,A., Baker,T.S. and Rossmann,M.G. (1993) Structure of a human rhinovirus complexed with its receptor molecule. *Proc. Natl Acad. Sci. USA*, **90**, 507–511.

Palmenberg,A.C. (1998) Polyprotein alignment of rhinoviruses website. Institute of Molecular Virology, University of Wisconsin at Madison, palmenberg@bioinformatics.bocklabs.wisc.edu.

Pevear,D.C., Fancher,M.J., Felock,P.J., Rossmann,M.G., Miller,M.S., Diana,G., Treasurywala,A.M., McKinlay,M.A. and Dutko,F.J. (1989) Conformational change in the floor of the human rhinovirus canyon blocks adsorption to HeLa cell receptors. *J. Virol.*, **63**, 2002–2007.

Pevear,D.C., Diana,G.D. and McKinlay,M.A. (1992) Molecular targets for antiviral therapy of the common cold. *Semin. Virol.*, **3**, 41–55.

Racaniello,V.R. (1996) Early events in poliovirus infection: virus–receptor interactions. *Proc. Natl Acad. Sci. USA*, **93**, 11378–11381.

Register,R.B., Uncapher,C.R., Naylor,A.M., Lineberger,D.W. and Colonno,R.J. (1991) Human–murine chimeras of ICAM-1 identify

amino acid residues critical for rhinovirus and antibody binding. *J. Virol.*, **65**, 6589–6596.

Rossmann,M.G. (1994) Viral cell recognition and entry. *Protein Sci.*, **3**, 1712–1725.

Rossmann,M.G. and Palmenberg,A.C. (1988) Conservation of the putative receptor attachment site in picornaviruses. *Virology*, **164**, 373–382.

Rossmann,M.G. *et al.* (1985) Structure of a human common cold virus and functional relationship to other picornaviruses. *Nature*, **317**, 145–153.

Rueckert,R.R. (1996) *Picornaviridae*: the viruses and their replication. In Fields,B.N., Knipe,D.M. and Howley,P.M. (eds), *Fields Virology*. Lippincott-Raven Publishers, Philadelphia, PA, Vol. 1. pp. 609–654.

Sack,J.S. (1988) CHAIN—a crystallographic modeling program. *J. Mol. Graph.*, **6**, 224–225.

Sherry,B., Mosser,A.G., Colonno,R.J. and Rueckert,R.R. (1986) Use of monoclonal antibodies to identify four neutralization immunogens on a common cold picornavirus, human rhinovirus 14. *J. Virol.*, **57**, 246–257.

Smith,T.J. *et al.* (1986) The site of attachment in human rhinovirus 14 for antiviral agents that inhibit uncoating. *Science*, **233**, 1286–1293.

Smith,T.J., Chase,E.S., Schmidt,T.J., Olson,N.H. and Baker,T.S. (1996) Neutralizing antibody to human rhinovirus 14 penetrates the receptor-binding canyon. *Nature*, **383**, 350–354.

Smyth,M., Tate,J., Hoey,E., Lyons,C., Martin,S. and Stuart,D. (1995) Implications for viral uncoating from the structure of bovine enterovirus. *Nature Struct. Biol.*, **2**, 224–231.

Staunton,D.E., Merluzzi,V.J., Rothlein,R., Barton,R., Marlin,S.D. and Springer,T.A. (1989) A cell adhesion molecule, ICAM-1, is the major surface receptor for rhinoviruses. *Cell*, **56**, 849–853.

Staunton,D.E., Dustin,M.L., Erickson,H.P. and Springer,T.A. (1990) The arrangement of the immunoglobulin-like domains of ICAM-1 and the binding sites for LFA-1 and rhinovirus. *Cell*, **61**, 243–254.

van de Stolpe,A. and van der Saag,P.T. (1996) Intercellular adhesion molecule-1. *J. Mol. Med.*, **74**, 13–33.

Wang,J. and Springer,T.A. (1998) Structural specializations of immunoglobulin superfamily members for adhesion to integrins and viruses. *Immunol. Rev.*, **163**, 197–215.

Yafal,A.G., Kaplan,G., Racaniello,V.R. and Hogle,J.M. (1993) Characterization of poliovirus conformational alteration mediated by soluble cell receptors. *Virology*, **197**, 501–505.

Zhao,R., Pevear,D.C., Kremer,M.J., Giranda,V.L., Kofron,J.A., Kuhn,R.J. and Rossmann,M.G. (1996) Human rhinovirus 3 at 3.0 Å resolution. *Structure*, **4**, 1205–1220.